Tellus (2004), 56B, 194–212
Printed in UK.

TELLUS

On the CO_2 exchange between the atmosphere and the biosphere: the role of synoptic and mesoscale processes

By DOUGLAS CHAN[1]*, CHIU WAI YUEN[3], KAZ HIGUCHI[1], ALEXANDER SHASHKOV[1], JANE LIU[2], JING CHEN[2] and DOUGLAS WORTHY[1], [1]*Meteorological Service of Canada, 4905 Dufferin Street, Toronto, Ontario, Canada M3H 5T4;* [2]*University of Toronto, Toronto, Ontario, Canada;* [3]*Earth System Research, Toronto, Ontario, Canada*

(Manuscript received 13 May 2003; in final form 21 January 2004)

ABSTRACT

Estimating global carbon fluxes by inverting atmospheric CO_2 through the use of atmospheric transport models has shown the importance of the covariance between biospheric fluxes and atmospheric transport on the carbon budget. This covariance or coupling occurs on many time scales. This study examines the coupling of the biosphere and the atmosphere on the meso- and synoptic scales using a coupled atmosphere–biosphere regional model covering Canada. The results are compared with surface and light aircraft measurement campaigns at two boreal forest sites in Canada (Fraserdale and BERMS).

Associated with cold and warm frontal features, the model results showed that the biospheric fluxes are strongly coupled to the atmosphere through radiative forcing. The presence of cloud near frontal regions usually results in reduced photosynthetic uptake, producing CO_2 concentration gradients across the frontal regions on the order of 10 parts per million (ppm). Away from the frontal region, the biosphere is coupled to the mesoscale variations in similar ways, resulting in mesoscale variations in CO_2 concentrations of about 5 ppm.

The CO_2 field is also coupled strongly to the atmospheric dynamics. In the presence of frontal circulation, the CO_2 near the surface can be transported to the mid to upper troposphere. Mesoscale circulation also plays a significant part in transporting the CO_2 from the planetary boundary layer (PBL) to the mid-troposphere. In the absence of significant mesoscale or synoptic scale circulation, the CO_2 in the PBL has minimal exchange with the free troposphere, leading to strong gradients across the top of the PBL. We speculate that the ubiquity of the common synoptic and mesoscale processes in the atmosphere may contribute significantly to the rectifier effect and hence CO_2 inversion calculations.

1. Introduction

One of the methods most often used to estimate the global distribution of terrestrial CO_2 sources and sinks in recent years utilizes inversions of atmospheric CO_2 measurements and related isotopes. Use of atmospheric CO_2 data has several advantages:

(1) Compared with the other two major carbon reservoirs (the oceans and the land biosphere), the atmosphere has been sampled for the longest time and with relatively wide spatial coverage.

(2) Atmospheric CO_2 measurements are relatively accurate and have been obtained on a regular timely basis, certainly sufficient to resolve seasonal variations.

(3) The atmosphere is coupled directly to both the oceans and the land biosphere, and the spatial and temporal behaviours of the latter two major carbon reservoirs are reflected in the observations of the CO_2 concentration field in the atmosphere.

Inversion calculations exploit these qualities of atmospheric CO_2 measurements through the use of atmospheric transport models, which in theory should provide a causative direct connection between the oceanic and land biospheric sources and sinks with observations at the CO_2 monitoring stations.

The inversion methodology has been also referred to as the top-down approach, because it employs a set of "global" measurements (i.e. data from a global network of surface stations, most of which are located at remote marine boundary layer sites) to infer regional to local source functions of CO_2. The focus of this approach has been to obtain estimates of magnitude and distribution of the terrestrial sink. A recent inversion study by Gurney et al. (2002) provides a summary of the results of a model comparison exercise called TransCom3 involving 16 atmospheric transport models from various research groups.

In order to make proper interpretation of the CO_2 measurements from the network of background monitoring stations in

*Corresponding author.
e-mail: douglas.chan@ec.gc.ca

terms of carbon land sources and sinks, we need to understand the processes by which the biospheric flux of CO_2 is communicated to the troposphere, and then eventually to these monitoring stations. In addition to various problems such as uniqueness of a model solution that depends on observing density and the resolution of the model source function, the inversion methodology faces problems related to the "rectifier effect" (Denning et al. 1996a,b). This effect is due to the existence of a covariance between the biospheric flux and atmospheric transport, and occurs on many space and time scales, from synoptic to global and annual. Physically, the rectifier effect is based on the idea that solar radiation drives both photosynthesis and thermal convection, and therefore photosynthesis and thermal convection have strong covariation on the diurnal and seasonal time scales. On the seasonal time scale, in a "fair weather" situation over the continent during the growing season, photosynthetic uptake is associated with a deep convective planetary boundary layer (PBL). This deficit CO_2 signal is mitigated by dilution in the deep PBL. In contrast, the shallow winter PBL traps the air enriched in CO_2 from the respiration efflux. This covariance may result in a time mean spatial concentration gradient in the atmosphere, as noted in global transport models with neutral biosphere fluxes (e.g. Denning et al. 1999; Gurney et al. 2002). Similar covariance occurs on the diurnal time scale. Unless we understand the details of the mechanism(s) of this covariance, it can lead to wrong estimates of biospheric CO_2 fluxes from inverting the background CO_2 measurements (Denning et al. 1999). There is a need to understand the various processes involved in scaling the variations in CO_2 concentration to regional CO_2 flux. In the present study, we address part of this issue by elucidating some aspects of the rectifier effect in the mid-latitude Northern Hemisphere by demonstrating the significance of the impact of synoptic scale and mesoscale atmospheric processes on a regional distribution of the atmospheric CO_2 field over Canada. We focus on the role of atmospheric processes on a time scale of 1–5 days. We emphasize the importance of the interaction between the atmospheric dynamics and the biospheric flux in non-"fair weather" conditions, and that uncoupling of the atmosphere and the land biosphere (as in global inversion models with a neutral biosphere) could lead to a biased estimates of biospheric flux.

The approach we take is relatively simple, although the technology we use is not. We employ a regional atmospheric dynamical model MC2 (the Mesoscale Compressible Community Model, Benoit et al. 1997) coupled interactively to an ecosystem model called BEPS (Boreal Ecosystem Productivity Simulator, Liu et al. 2002) for Canada. The MC2–BEPS coupled model is used to simulate atmospheric CO_2 and meteorological measurements taken during intensive measurement campaigns (which included aircraft measurements) at two boreal sites (Fraserdale in northern Ontario, and BERMS (Boreal Ecosystem Research and Monitoring Sites, http://berms.ccrp.ec.gc.ca/) in Saskatchewan, Canada). After verification of the coupled model, we examine the interaction of the biosphere and the atmosphere, as well as the atmospheric mixing processes including some weak frontal passages during the intensive campaigns. Then we investigate the atmospheric mixing processes of CO_2 during more notable synoptic frontal system.

2. Model description

2.1. MC2

A detailed description of the MC2 model is found in Benoit et al. (1997). Therefore, only a brief description is given here. MC2 is a 3-D limited-area fully compressible model with a semi-implicit semi-Lagrangian time scheme. The model can achieve finer resolution by nesting into subdomains. Dynamically, MC2 solves a full set of Navier–Stokes equations for the atmosphere subject to the boundary conditions of the limited area domain. The coordinate system used is terrain following with topography taken into account using the Gal-Chen height coordinate (Gal-Chen and Somerville, 1975).

Thermodynamics in the model is treated by the physics package described in Benoit et al. (1989), Mailhot et al. (1989) and Mailhot (1994). The package includes many important PBL processes. Modelling of the diffusive processes in the PBL is based on turbulent kinetic energy theory, while in the stratified surface layer it is based on similarity theory (Benoit et al. 1989). There is a shallow convection scheme (Mailhot, 1994) to simulate the radiative and destabilization effects of shallow non-precipitating clouds at the top of the PBL. Deep convection uses the Kuo-type deep convection scheme (Kuo, 1974). The surface temperature is based on a heat budget (force-restore) method (Deardorff, 1978). Solar (Fouquart and Bonnel, 1980) and infrared (Garand, 1983) radiation schemes are interactive with clouds. This feature plays an important role in the interaction between the atmosphere and the biosphere and will be discussed later in the result section.

In this study, the domain of MC2 is shown in Fig. 1. It covers North America with a polar stereographic projection, with a horizontal resolution of 20 km, true at 60°N. The vertical domain has 25 levels going from the surface to 20 km height in the Gal-Chen coordinate, with nine levels in the first kilometre above the surface to resolve the PBL. The time step is 6 min. The initial and lateral boundary conditions are supplied by the Canadian Meteorological Centre (CMC) analysis. The model simulations of the intensive campaign periods (about 5 days per campaign) are reinitialized each day at 0 UT (Universal Time) to maintain comparability of the model results and meteorological observations.

2.2. BEPS

The Boreal Ecosystems Productivity Simulator (BEPS) model is described in Liu et al. (1997, 2002). Briefly, BEPS is a process model developed to simulate ecosystem productivity from small to large scales ($\sim 10^8$ km^2 or continental scale). BEPS was built based on a site-level ($\sim 10^{-2}$ km^2) process model,

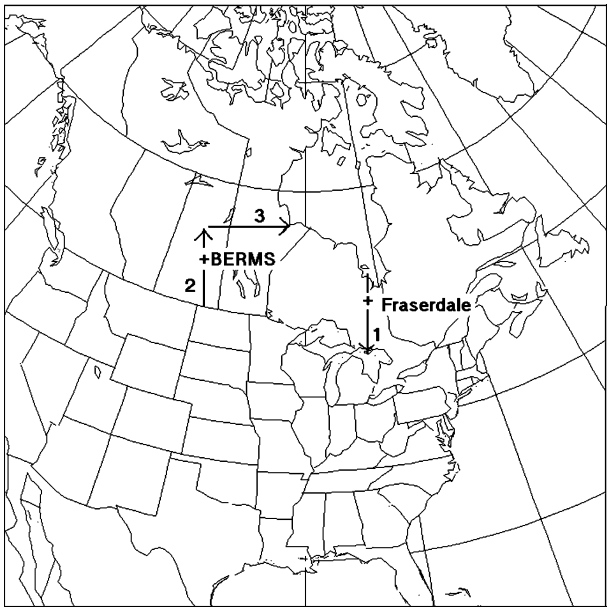

Fig 1. Map of the model domain of MC2. Also shown are the locations of the Fraserdale and BERMS measurement sites, as well as the locations of the three vertical cross-sections of the model results discussed in Section 3. The direction of the arrow indicates the left to right orientation in the vertical cross-section plots.

FOREST-BGC (Running and Coughlan, 1988). Scaling from site to region was achieved through incorporating spatial data from various sources. The data include leaf area index (LAI) derived from advanced very high resolution radiometer (AVHRR) satellite measurements (Chen and Cihlar, 1996; Cihlar et al. 1997), land cover map data compatible with AVHRR (Cihlar et al. 1999) and the GIS soil database (Shields et al. 1991). The temporal interval is 10 to 11 days for LAI during the growing season. The land cover map and soil data are both variant spatially but invariant temporally in 1 year.

Significant modifications of BEPS from FOREST-BGC include the canopy radiation calculation (Liu et al. 1997) and canopy photosynthesis calculation (Liu et al. 2002). The rate of photosynthesis is critically dependent on the amount photosynthetic active radiation (PAR) absorbed by the canopy. BEPS takes into account the fraction of PAR (FPAR) absorbed by the canopy following the methods established by Chen (1996a,b). The absorbed PAR is separated into sunlit and shaded leaves and the photosynthesis is calculated separately for these two groups of leaves by the within-canopy spatial scaling scheme (Liu et al. 2002).

With the meteorological forcing that includes shortwave radiation, temperature, humidity and precipitation, as well as vegetation and soil data, BEPS computes net primary productivity (NPP), net ecosystem productivity (NEP), transpiration, evapotranspiration, soil water content and other variables that characterize the ecosystem–atmosphere exchange. For the present study the domain of BEPS is Canada. The coordinate system used is the Lambert conformal conic projection with a resolution of 1 km.

2.3. Coupled model

In this study, the two models, MC2 and BEPS, were coupled together. The coupling permitted examination and analyses of the exchange and interaction between the biosphere and the atmosphere. There were some technical issues in the coupling exercise. The domain of MC2 uses the polar stereographic map projection with a horizontal resolution of 20 km and a time step of 6 min, while BEPS employs the Lambert conformal conic projection with a horizontal resolution of 1 km and a time step of 1 h.

To achieve coupling, the two models were modified. A tracer equation with advection, diffusion and surface source terms was added to MC2 to model the atmospheric CO_2 field. BEPS was modified from a daily time step to an hourly time step. The procedure of coupling was as follows. First, the MC2 model was executed to generate the hourly meteorological fields of surface solar radiation, temperature, humidity and precipitation. These MC2 outputs were then converted from the polar stereographic to the Lambert conformal conic projection and bilinearly interpolated to the higher horizontal resolution of BEPS. BEPS was then driven with the MC2 meteorological outputs to yield hourly NEP over Canada at a resolution of 1 km. The high-resolution outputs of BEPS were then summed and remapped to yield NEP over Canada on the 20 km resolution polar stereographic domain of MC2. Outside Canada, NEP was set to nil. The hourly BEPS NEP fluxes were interpolated onto the 6 min time step of MC2. Finally, MC2 was run again with the NEP surface fluxes to simulate atmospheric evolution of the CO_2 tracer. In this study, the anthropogenic and oceanic CO_2 fluxes were not included.

The CO_2 field in MC2 was initialized with a uniform concentration (0 parts per million (ppm)). The initial concentration served as a reference for the time evolution of the CO_2 field. Thus 0 ppm in the model corresponded to the mean background tropospheric CO_2 concentration (approximated by the CO_2 concentration from Alert (82°27′ N, 62°31′ W), Canada), which is about 355 ppm in the observations for the July 2000 campaign at Fraserdale and about 360 ppm for the July 2002 campaign at BERMS. The CO_2 field at the MC2 model boundary was fixed at 0 ppm. Since the MC2 model was reinitialized with CMC analysis following each 1-day simulation, the CO_2 field in MC2 was saved at the end of each 1-day simulation and used as the initial field for the following 1-day simulation. With the model horizontal resolution of 20 km, we will limit the discussion to the synoptic and mesoscale processes resolvable in the model.

3. Model results and discussion

With a brief description of the regional atmospheric model (MC2) and the biospheric flux model (BEPS) completed, we

now focus on the verification and validation of the coupled model and its ability to simulate the exchange processes between the biosphere and the atmosphere.

With the exception of the years 1997, 1998 and parts of 1999, continuous measurements of atmospheric CO_2 and meteorological conditions have been made since 1990 on a 40 m tower at Fraserdale (50°N, 81°W), located in a boreal forest site in northern Ontario, Canada (Higuchi et al. 2003). The surrounding ecosystem is dominated mainly by black spruce, followed by poplar, jack pine and birch trees. During the period 1998–2000, the regular surface measurements were supplemented with six intensive field campaigns, mostly during the growing season.

In 2002, to supplement the existing CO_2 flux measurement programme at the BERMS site in Prince Albert, Saskatchewan, Canada (54°N, 105°W), we initiated the measurement of continuous CO_2 concentration on the eddy-covariance CO_2 flux tower at the old black spruce (OBS) location. One intensive aircraft campaign in July 2002 was performed over the BERMS site. The locations of Fraserdale and BERMS are shown in Fig. 1.

On average, each campaign lasted for about 4–5 days, and consisted of surface flask samples for isotopic analyses (as well as for other trace gases) and vertical aircraft profiling that included *in situ* CO_2 and meteorological measurements, as well as flask samples for trace gases and CO_2 isotopes.

For the purpose of this study, we used the data gathered during the last two campaigns. These campaigns have the most complete data coverage and covered the effects of changing air masses. One campaign was at Fraserdale for the period of 25–29 July 2000 (corresponding to the Julian days 207 to 211), and the second campaign was at BERMS for the period of 8–12 July 2002 (corresponding to the Julian days 189 to 193). The coupled model was evaluated by comparing the model simulation with the surface and aircraft observations. The results for the July 2000 campaign at Fraserdale are presented below. A similar degree of agreement between model results and observations was obtained for the July 2002 campaign at BERMS (not shown).

3.1. *Model simulations of CO_2 measurements at Fraserdale*

MC2 computes meteorological fields at different heights. Temperature and specific humidity at the 1.5 m level (which we will call the surface) computed by the model will be compared with the observations taken at the same level (Figs. 2 and 3). Atmospheric CO_2 at the first model level of 15 m will be compared with the CO_2 data obtained at the 20 m level on the tower (Fig. 4). The time series in Figs. 2–4 are plotted using UT. The relationship to the local time in July at Fraserdale is UT minus 4 h. The atmospheric CO_2 concentration was monitored at the 20 and 40 m levels. The CO_2 concentration field in MC2 is generated by the BEPS net CO_2 flux, driven by the meteorology of MC2. Comparisons of model results with the aircraft vertical profiles of CO_2 and potential temperature are shown in Figs. 5 and 6.

Figure 2 shows the time evolution of temperature at the surface (1.5 m). There was a strong diurnal cycle driven mainly by the radiative forcing cycle of daytime heating and night-time cooling. Also, there was a slower variation over several days governed by the movement of large-scale air masses. During this period with the passage of a weak cold front, the warm air mass (days 206–209) was replaced by a cooler air mass (days 210–211). The model was able to simulate these features. This gives a measure of the model's ability to simulate the surface energy fluxes (important for the correct diurnal cycle) and large-scale atmospheric dynamics (important for the advection of air

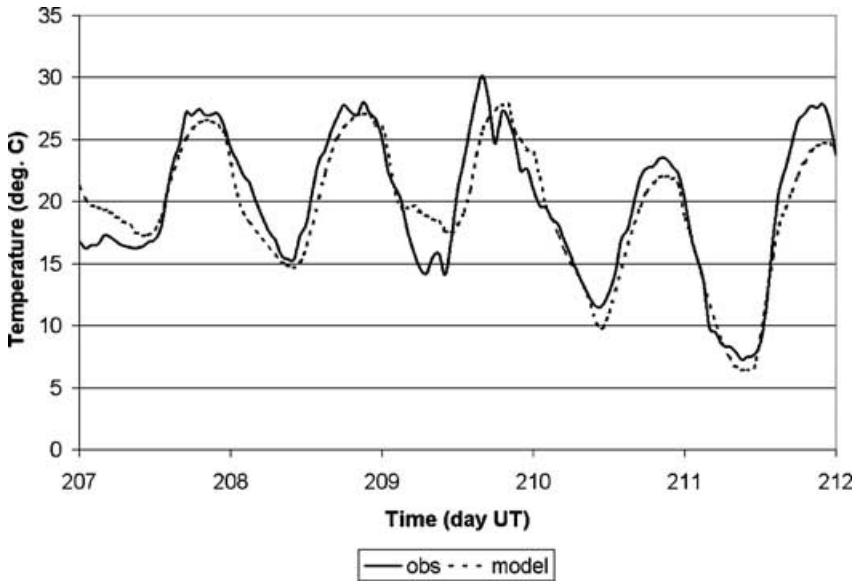

Fig 2. Fraserdale surface temperature time series for model and observation during the July 2000 measurement campaign. The uncertainty in the observed temperature is about 0.2 °C.

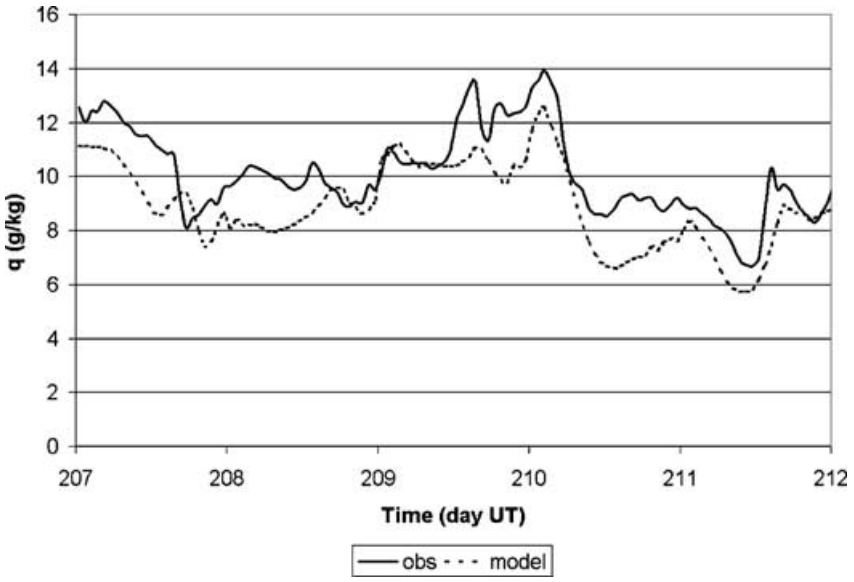

Fig 3. Fraserdale model and observed surface specific humidity q (g kg^{-1}) time series for the July 2000 campaign. The uncertainty in the observed specific humidity is about 0.2 g kg^{-1}.

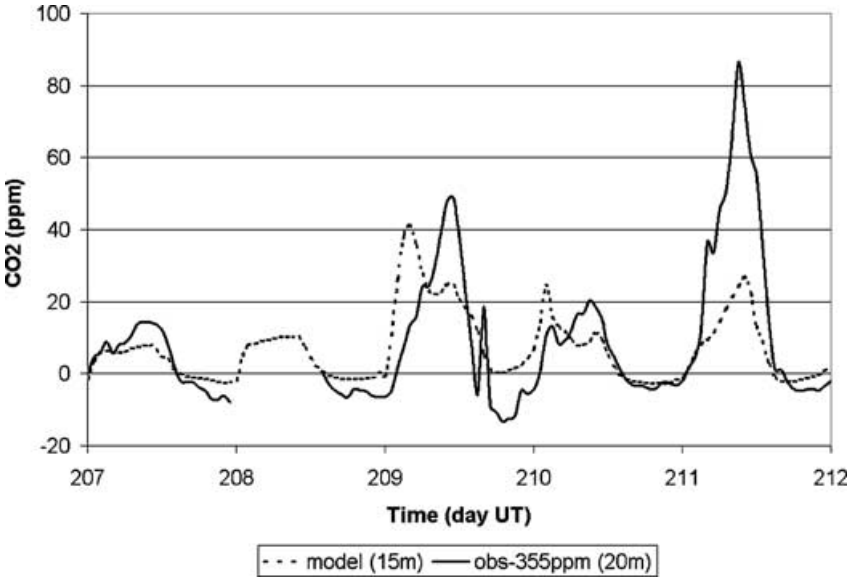

Fig 4. Fraserdale CO_2 concentration (in ppm) time series for the July 2000 campaign. Model results are for the 15 m level, measurements from the 20m level. The uncertainty in the tower-observed CO_2 concentration is about 0.1 ppm.

masses). There is general agreement between the model results and observations. The observed temperature record shows more short time scale variability than the model results, reflecting the existence of small-scale processes not captured by the model with horizontal resolution of 20 km.

Figure 3 shows the surface specific humidity at the 1.5 m level. Model results and observations are in general agreement, though the model results are 1–2 g kg^{-1} drier. There are fewer diurnal features in this field. As was the case with the surface temperature, the model does not capture all the short time scale variability present in the observation. The model does, however, show the build-up of surface moisture before the passage of the weak cold front on day 209 and the reduction of surface moisture after the passage. The arrival of the drier air after the passage of the weak cold front over Fraserdale was at ∼0 UT, day 210.

Figure 4 shows the CO_2 concentration of the model at 15 m and the observation at 20 m. Both model results and observations showed strong diurnal cycles in the CO_2 concentration. The model results also compared well with the day to day variability of the diurnal cycle (particularly before the passage of the weak cold front). The day to day variability of the diurnal cycle is a strong function of the characteristics (strength and thickness) of the night-time stable layer. Typically, a stable layer formed by radiative cooling will trap the night-time respired CO_2 near the surface and build up a large night-time peak in the CO_2 concentration. The peak collapses in the morning with the onset of photosynthetic draw-down and the breakdown of the surface

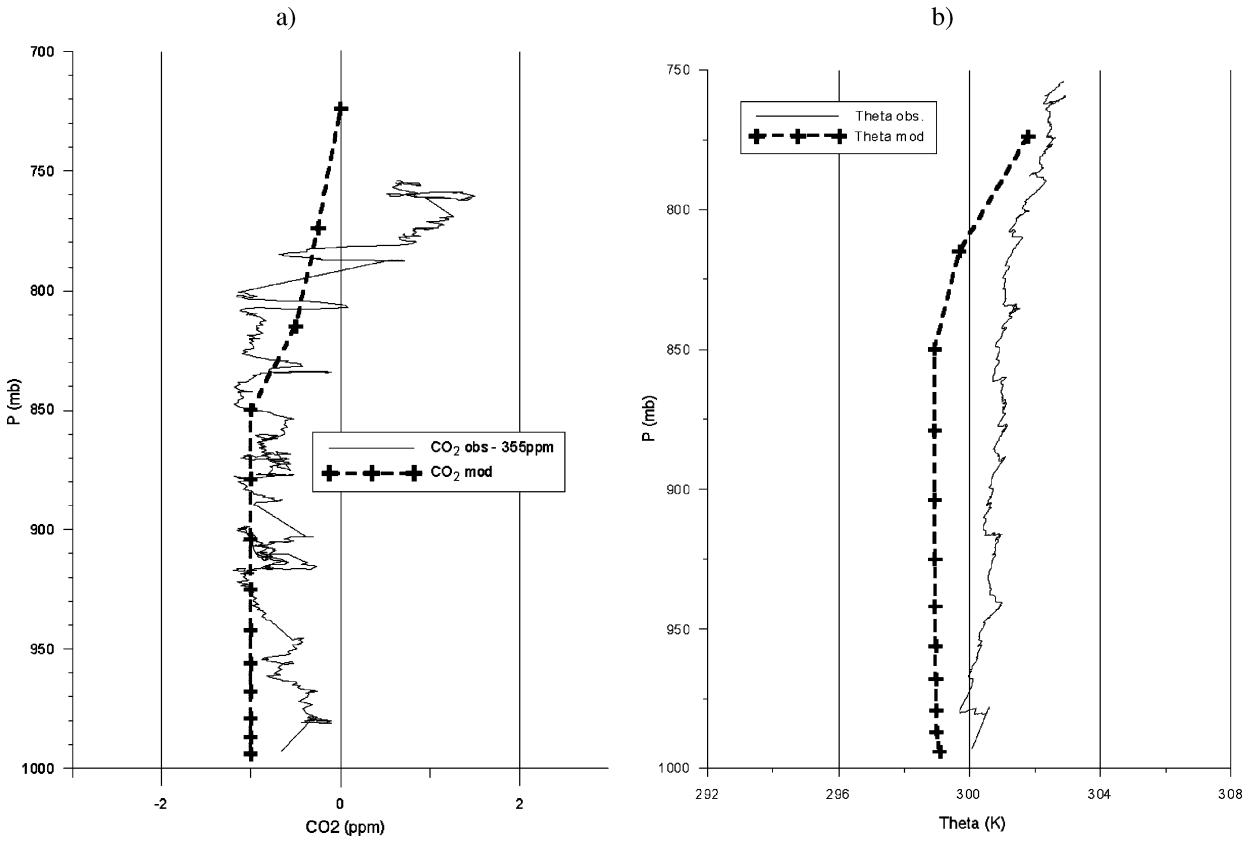

Fig 5. Vertical profiles of the model and observed CO_2 (a) and potential temperature θ (b) for the afternoon of day 208 at Fraserdale (observation from an ascending profile). The uncertainty in the CO_2 concentration is about 0.3 ppm, and about 0.2 K for potential temperature.

inversion layer. Different intensities of radiative cooling and subsidence will result in strong inversion in a shallow layer with a corresponding large nocturnal CO_2 maximum, or weaker inversion in a deeper layer with a smaller nocturnal CO_2 maximum. These processes are evident in the model (Stull, 1993; Bakwin et al. 1995, 1998).

The model results compared well with the observations from day 206 to day 209. After the passage of the weak cold front, the difference between model results and observations became large, especially on day 211. A possible factor affecting the model results was the strong radiative cooling in the cool clear nights. Fraserdale cooled to ∼7 °C on day 211, compared with ∼15 °C on day 209. Since MC2 has only two levels in the lowest 100 m (15 m and 60 m), the shallow surface layer was not sufficiently well resolved to yield the observed strong CO_2 maximum. The highly stable surface layer was also evident in the observed CO_2 concentration. There was a strong gradient in the CO_2 concentration between the 20 and 40 m levels (not shown). Also, the near-surface wind speed generally decreases at night (to as slow as 2 m s^{-1}). With the weak wind, the observed CO_2 at the tower may be strongly influenced by local variations in microscale transport and biospheric flux variations. Heterogeneity near the tower, including a large reservoir, river valley and hills, may influence the measurements. Such small-scale processes are not simulated in the model.

Aircraft measurements at Fraserdale consist of morning and afternoon vertical profiles to a 3 km height of continuous CO_2 concentrations and meteorological data, as well as flask samples collected for CO_2 isotopes and other trace gases. Here we focus on the change in the vertical structures of CO_2 and potential temperature following the passage of a weak cold front. Figure 5 shows the afternoon (20 UT, or 16 h local time) vertical profiles of CO_2 concentration (Fig. 5a) and potential temperature (Fig. 5b) for day 208, when Fraserdale was in the warm air mass. The afternoon well-mixed layer reached a height of ∼820 mb. Figure 6 shows the vertical profiles of CO_2 concentration and potential temperature for day 210 at 20 UT (16 h local time), when Fraserdale was in the cool air mass. The afternoon well-mixed layer reached only about 900 mb, although solar forcing, and thus surface heating, was greater on day 210 when Fraserdale was in the clear cool air.

These results show that atmospheric dynamics of the different air masses play an important role in the boundary layer dynamics. The strong stability of the subsiding cool air can cap the development of a well-mixed layer, while the large-scale lifting (or weaker subsidence) of the warm sector air, generally with some

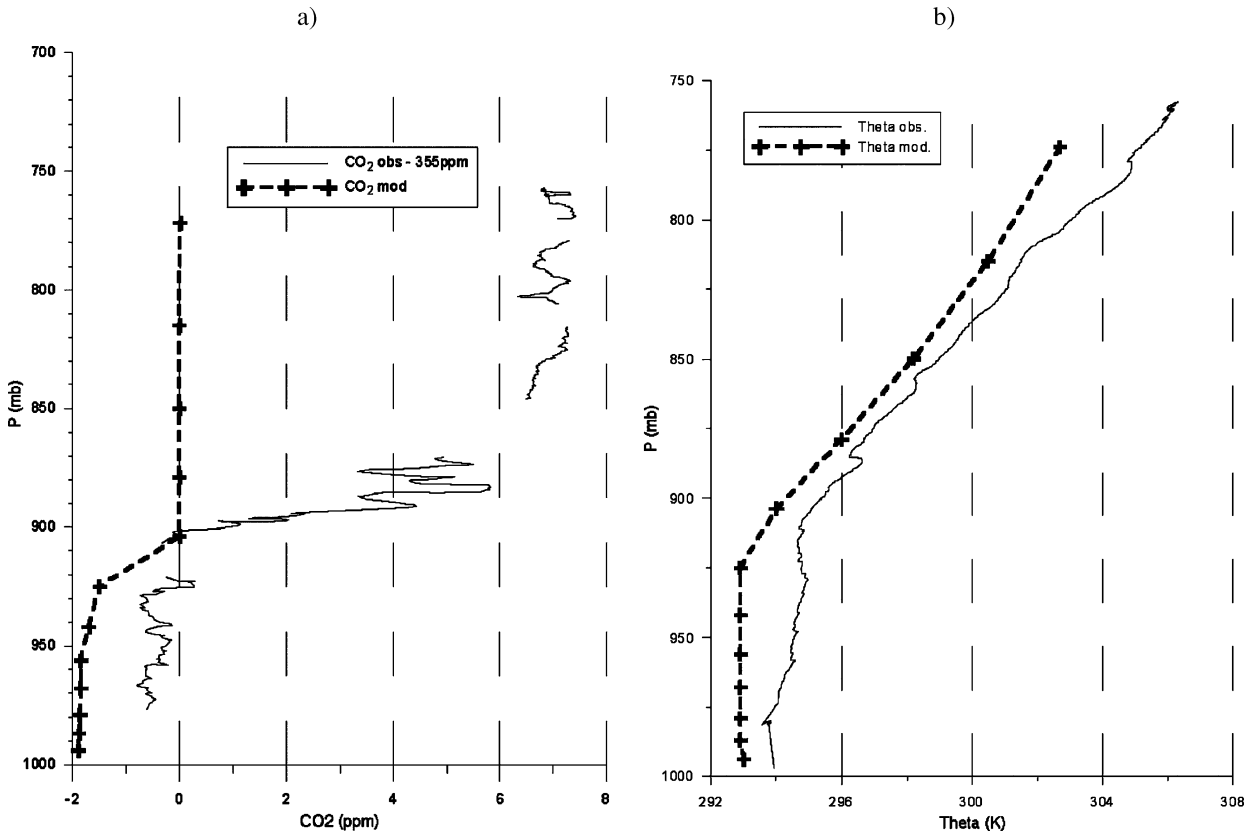

Fig 6. Vertical profiles of the model and observed CO_2 (a) and potential temperature θ (b) for the afternoon of day 210 at Fraserdale (observation from an ascending profile). The uncertainty in the CO_2 concentration is about 0.3 ppm, and about 0.2 K for potential temperature.

cloud activities, enables the PBL to reach a thickness of twice that in the cool air case. Thus synoptic scale dynamics could operate in an opposite sense to the PBL dynamics described by the diurnal or seasonal rectifier effects. The effects of synoptic scale dynamics on the PBL development are comparable to the seasonal rectifier effect. Note that in Figs. 5a and 6a, the differences between the modelled and the observed CO_2 can be quite large in the free troposphere. This indicates that the air in the free troposphere retains the history of past interaction, which was not taken into account in our model initialization process for CO_2. Thus long-range transport may play an important role in the local CO_2 budget. In contrast, the simulated vertical profiles of the potential temperature (Figs. 5b and 6b) agree relatively well with the observations. This is a result of the 24-h updating of the model meteorology with the observation from CMC.

Another interesting contrast between Figs. 5a and 6a is the vertical gradient of CO_2 between the PBL and the free troposphere. Observation on day 208 (Fig. 5a) shows a relatively gradual transition from the PBL to the free troposphere; the model produces a vertical CO_2 profile that is in good agreement with the observed profile. However, on day 210 (Fig. 6a), the PBL-free troposphere gradient shows a large sharp increase of about 8 ppm in a shallow layer located near the 900 mb level. The model is able to reproduce the height and the sharpness of the gradient but not its magnitude. This is due mainly to the issue of initialization of the CO_2 field in the model, as mentioned in the above paragraph. Another contributing factor is the limited model vertical resolution. Both model and observation show a sharp gradient across the PBL in Fig. 6a. The contrast in the vertical profiles between days 208 and 210 indicates there are different exchange processes operating between the PBL and the free troposphere on different days. These processes will be discussed in Section 3.3.

The comparative results shown in Figs. 2 to 6 demonstrate that the coupled model is capturing reasonably well the exchange of the biosphere and the atmosphere as reflected in the evolution of the diurnal cycles of CO_2 concentration and meteorology. The model is also capturing the variability of the exchange between the PBL and the free troposphere in different air masses. In the next section, the synoptic scale effects are explored in detail.

3.2. Model simulations of CO_2 variation on the synoptic scale

In atmospheric transport, the dominant factor driving the atmospheric circulation is the equator-to-pole contrast in solar forcing, with the resultant horizontal temperature gradient or baroclinicity. In mid-latitudes, baroclinic instability on the synoptic scale ($\sim$1000 km) leads to the formation of baroclinic waves

and frontal systems. In this subsection, we examine the effects of these synoptic frontal systems on the coupling of biospheric CO_2 flux and atmospheric transport. A typical case of a synoptic event has a horizontal potential temperature gradient $\Delta\theta \sim 10$ K, with a horizontal length scale $\Delta x \sim 1000$ km and a time scale $\Delta t \sim 10$ days.

The following sections will present a few cases of synoptic systems to illustrate a typical picture (showing the similarity and the ubiquity of the features) of the atmosphere–biosphere interaction, as well as the differences between the cases.

3.2.1. Weak cold frontal passage at Fraserdale. During the July 2000 campaign, there was a passage of a weak cold front on day 209 at Fraserdale (at ∼20 h local time or 0 UT, day 210). With a demonstrated ability of the model to simulate the CO_2 evolution during this period, our first case study of the atmospheric distribution of CO_2 introduced into the PBL by the BEPS biospheric flux was this cold front. Figure 1 shows three 800 km long lines indicating the locations of the vertical cross-sections that will be discussed in this and the following sections. The first cross-section (line 1) runs from James Bay to Lake Huron, with Fraserdale located at the 200 km point on the distance scale in the cross-section.

The evolution of the frontal passage and its effects on the CO_2 field can be seen in the time evolution of the model results. We will show the evolution of the interaction and transport by presenting the model results for before and after the frontal passage. Figure 7 shows the vertical cross sections for potential temperature θ (Fig. 7a), CO_2 concentration (Fig. 7b) and specific humidity q (Fig. 7c) for day 209, 18 UT (14 h local time), before the frontal passage at Fraserdale. Figure 8 shows the vertical cross sections for potential temperature θ (Fig. 8a), CO_2 concentration (Fig. 8b) and specific humidity q (Fig. 8c) for day 210, 18 UT, after the frontal passage.

The weakness and shallowness of the cold front could be seen in the vertical cross-sections of the potential temperature field before and after the passage of the front (Figs. 7a and 8a respectively). Figure 7a shows the θ field for the warm sector (day 209, 18 UT) before the frontal passage. The frontal passage occurred at about 0 UT, day 210. The PBL is the layer of well-mixed air with constant vertical θ. Near Fraserdale, the PBL reached up to about 800 mb. Also visible in both Figs. 7a and 8a is the effect of the cold water at the left (James Bay) and right (Lake Huron) ends of the cross-section, resulting in very shallow stably stratified surface layer. In Fig. 8a (day 210, 18 UT), the surface cold front or the 299 K θ contour (indicating the leading edge of the cold air mass) has reached the 500 km point in the cross-section. The difference in the PBL ahead of and behind the front is clear. In the warm sector ahead of the cold front, the well-mixed PBL reached about 850 mb. In contrast, the cold sector PBL reached only about 920 mb under general subsidence.

Figure 7b shows the vertical cross-section of atmospheric CO_2 before (day 209, 18 UT) the passage of the front. In the warm sector, the PBL CO_2 was convectively well-mixed to about 800 mb,

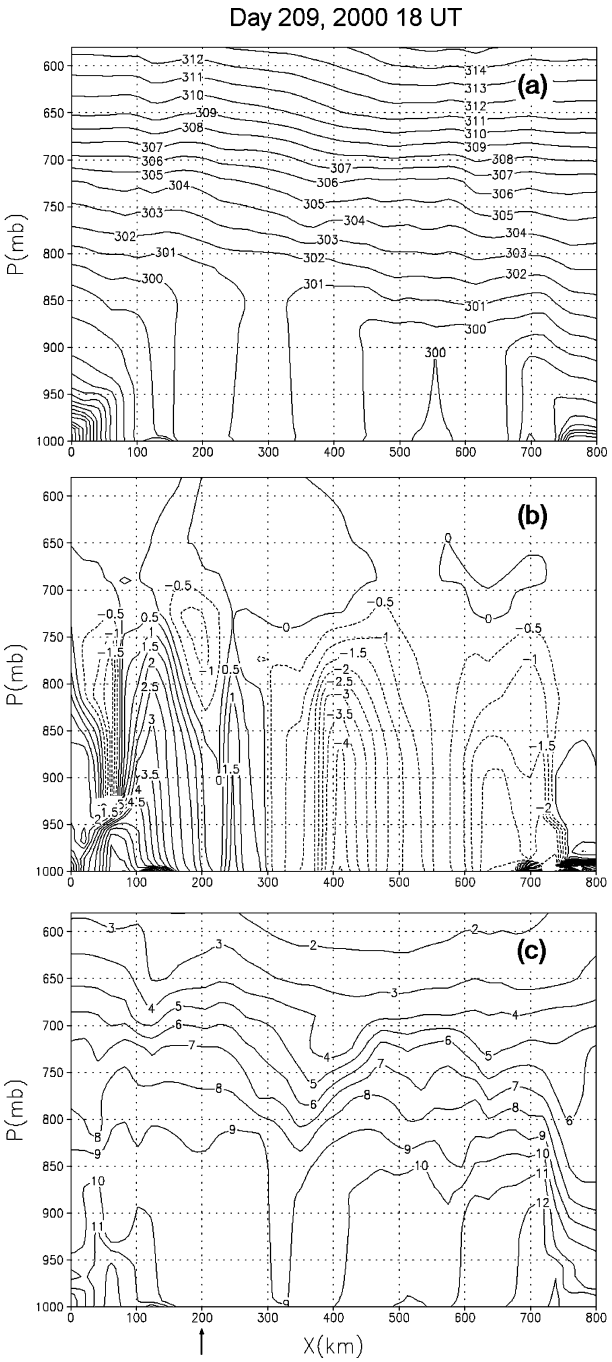

Fig 7. Vertical cross-sections of (a) potential temperature (K), (b) CO_2 (ppm) and (c) specific humidity q (g kg^{-1}), near Fraserdale (denoted by the arrow at 200 km) before the passage of the cold front.

but the CO_2 continued to mix upward to above 750 mb. Processes responsible for this significant transport of CO_2 from the PBL to the mid-troposphere will be discussed in Section 3.3.

On the following day at 18 UT (Figure 8b), the weak cold front had passed over Fraserdale (moving from left to right in the cross-section) and was located at about the 500 km point on

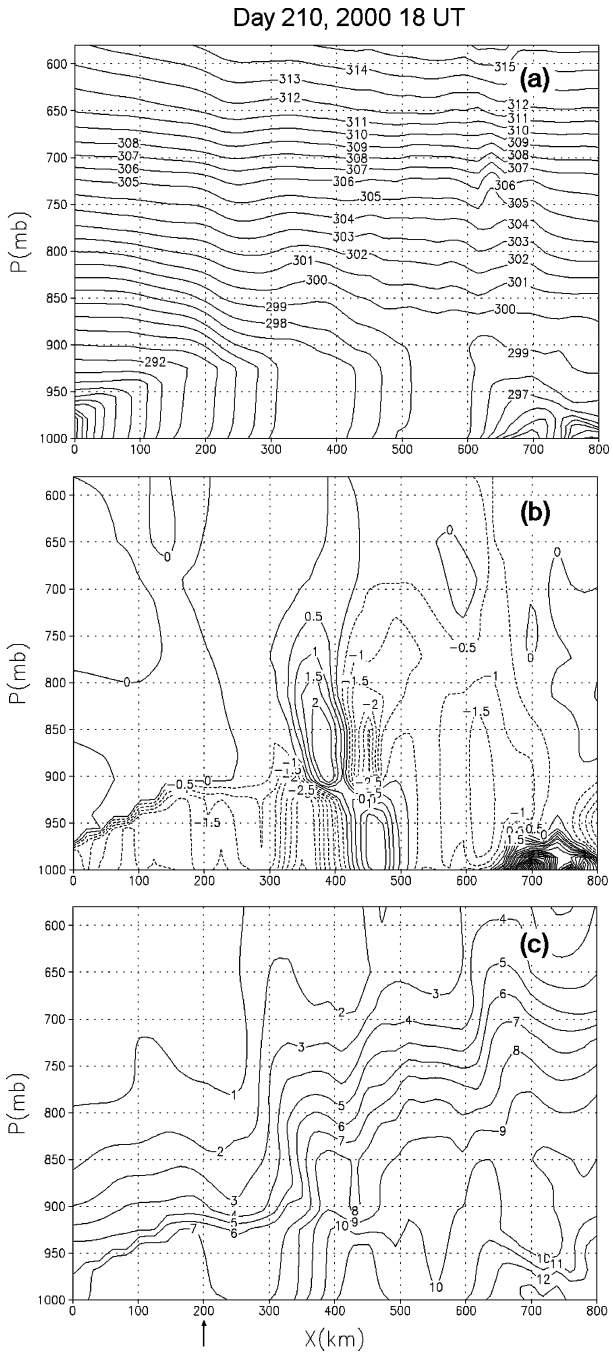

Fig 8. Vertical cross-sections of (a) potential temperature (K), (b) CO_2 (ppm) and (c) specific humidity q (g kg^{-1}), near Fraserdale (denoted by the arrow at 200 km) after the passage of the cold front.

the distance scale in the cross-section. The cold front pushes the warm air ahead of it and forces it to rise above the cold air along the frontal surface. If there is sufficient moisture in the air, then the rising air condenses. This has two effects:

(1) Diabatic heating from condensation enhances the upward flow of CO_2 along the cold front. Sometimes, the heating produces enough buoyancy to overcome the stable stratification leading to enhanced vertical transport.

(2) Clouds associated with the diabatic heating reduce solar radiation at the surface and consequently reduce photosynthesis. This leads to higher concentration of CO_2 under the frontal cloud band.

These effects are visible as a cold frontal band of air with higher CO_2 concentration reaching up to about 700 mb. The first effect due to diabatic heating is visible as the band of air with high CO_2 concentration rising along the sloping front to about 900 mb, then almost vertically to about 700 mb.

Ahead of the cold front (right side of the 500 km mark in Fig. 8b), the warm sector continued to exhibit deeply mixed PBL. In contrast, in the cold sector behind the front the PBL with well-mixed CO_2 reached only up to about 900 mb and is sharply capped by strong vertical CO_2 gradient. This is consistent with the frontal features shown in the θ cross-section.

Besides the frontal features, these figures also show that there are significant mesoscale features. In the warm sector, Fig. 7b shows horizontal variations in the CO_2 concentration in the PBL of the order of 5 ppm per 100 km. The dynamics of these features will be discussed in Section 3.3.

The transition from the warm air to the cold air is also visible in the time sequence of vertical cross-sections of the specific humidity field shown in Figs. 7c and 8c for before and after the frontal passage, respectively. Figure 7c shows the q field with little synoptic-scale gradient indicating that the cold front has not entered into the cross-section, while Fig. 8c shows a significant gradient across the cold front, with drier air in the cold sector. Both figures show noticeable mesoscale features in the warm sector. These mesoscale features extend from the PBL into the free troposphere. In contrast, the cold sector PBL air is confined within the PBL (Fig. 8c). These features show that the atmospheric transport processes are similar for the CO_2 and q fields. The mesoscale dynamics of these features will be discussed in Section 3.3.

These results are qualitatively comparable to the campaign aircraft profiles of CO_2 concentrations at Fraserdale shown in Fig. 9. Each row in the figure shows the morning (from 13–15 UT) and afternoon (from 19–21 UT) vertical profiles for the same day. For each flight, there are up to four profiles corresponding to a sequence of ascents and descents, with each ascent or descent taking approximately 30 min. The profiles follow the rainbow colour order to denote the time sequence. Thus the first ascent is plotted in red, the following descent is plotted in orange, the next ascent in green and the final descent in blue. The CO_2 concentration from the tower measurement is plotted as the lowest point of each profile. The observations were not taken on 27 July (day 209), the day of the frontal passage. However, as noted in Section 3.1, the sequence of the profiles shows the shallow PBL in the cold sector with large gradients across the PBL-free troposphere boundary (the afternoon profiles on 28 July (day 210)),

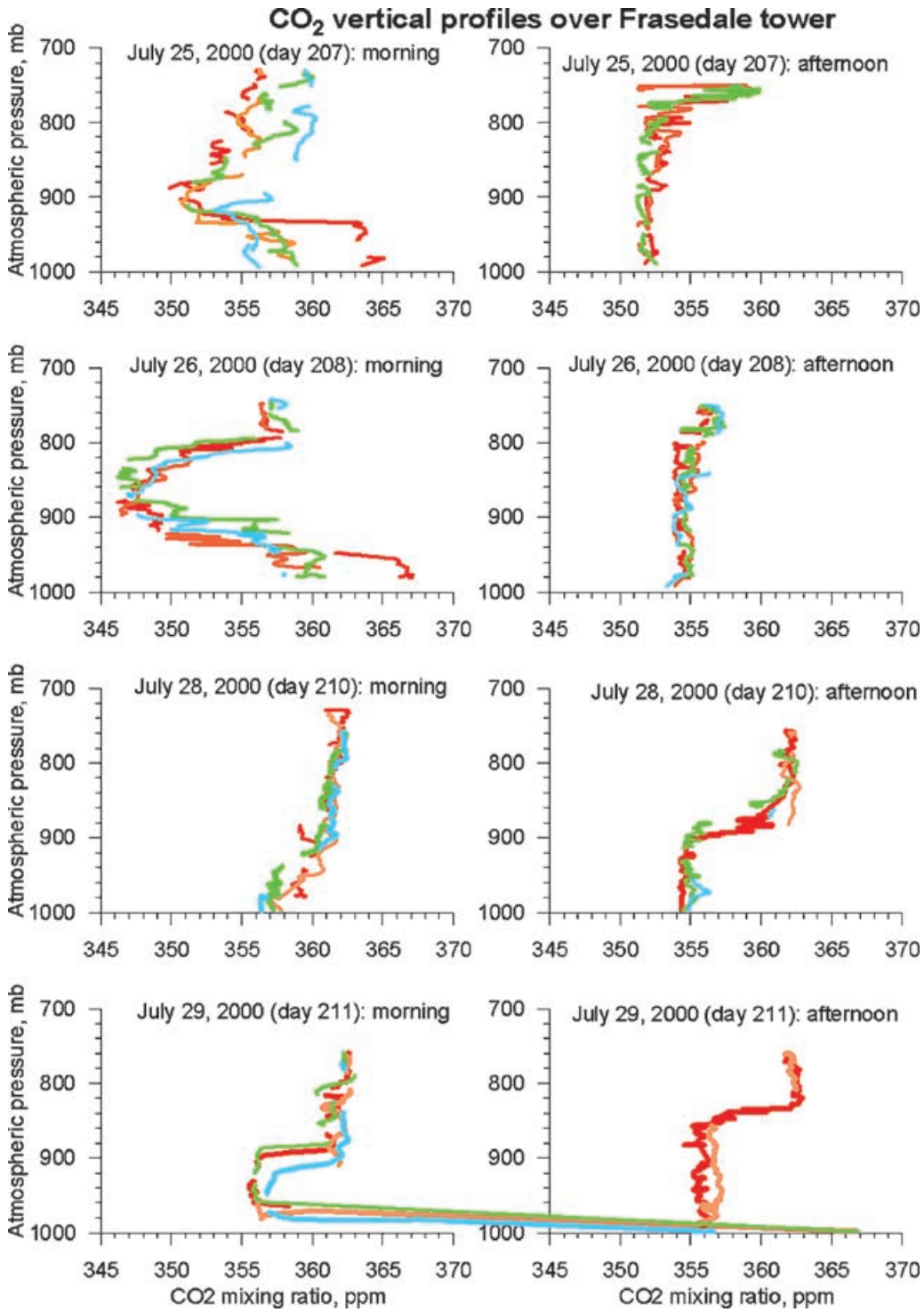

Fig 9. The sequence of aircraft vertical profiles for the July 2000 campaign. Each row shows the morning (from 13–15 UT) and afternoon (from 19–21 UT) vertical profiles for the same day. For each flight, there are up to four profiles corresponding to a sequence of ascents and descents, with each ascent or descent taking approximately 30 min. The profiles follow the rainbow colour sequence to denote the time sequence. Thus the first ascent is plotted in red, the following descent is plotted in orange, the next ascent in green and the final descent in blue. The surface tower measurement at the corresponding time is plotted as the lowest point of each profile. The uncertainty in the aircraft CO_2 measurement is about 0.3 ppm.

in contrast to the deep warm sector PBL with small transitional gradients (the afternoon profiles on 26 July (day 208)). Within the warm sector, the sequence of morning profiles on 25 July (day 207) showed the advection of air with a higher CO_2 concentration to Fraserdale above the 900 mb level. For a typical wind speed of 10 m s^{-1}, the profiles capture the movement of air with a CO_2 gradient of about 5 ppm per 100 km. By comparing the 25 July (day 207) afternoon profiles with the 26 July (day 208) morning profiles, there is evidence of an overnight advection of air with a CO_2 concentration about 5 ppm lower in the PBL residual layer (between 900–800 mb). These mesoscale variations of CO_2 are comparable to the mesoscale variations simulated in the model (see Figs. 7b and 8b).

There are prominent surface maxima in the CO_2 profiles on the morning of 29 July (day 211). On that morning, fog formed in the stable surface layer produced by the strong overnight radiative cooling. The ground fog delayed the surface warming in the morning and the destruction of the stable night-time surface layer. Also, the fog reduced the surface solar radiation and photosynthetic draw-down. Thus the large build-up of night-time respired CO_2 in the stable surface layer remained visible as the large surface CO_2 maxima in the figure. The surface CO_2 values (from the tower data) for the profiles were about 400 ppm.

The simulated variation in the CO_2 field is consistent with the simulated CO_2 flux in response to atmospheric forcing. Figure 10 shows the evolution of the CO_2 flux at the $20 \times 20\,km^2$ grid point containing Fraserdale as simulated by BEPS. On days 210 and 211 (after the passage of the weak cold front), Fraserdale, in the cooler and drier air mass, showed strong draw-down of CO_2. Note that a draw-down of CO_2 from the atmosphere to the biosphere is indicated by a negative NEP in Fig. 10. The daytime net flux (from sunrise to sunset) for day 210 was -9.0×10^{-3} kg C m^{-2}, indicating a strong draw-down of CO_2. On the day of frontal passage (day 209), under cloudy conditions, Fraserdale acted as a source of CO_2 with total daytime net flux of 4.0×10^{-3} kg C m^{-2}. While before the frontal passage (days 207 and 208), the partial cloudiness in the warm sector reduced the total daytime net flux to about -1.4×10^{-3} kg C m^{-2} (a slight draw-down). As the daytime flux strength could change from hour to hour and from day to day, the flux variations lead to the variations in the simulated CO_2 concentration on the different horizontal scales. There is less variation visible in the night-time flux, although the figure shows reduced soil respiration at night in the cooler air mass.

3.2.2 Weak warm frontal passage at BERMS. During the July 2002 aircraft campaign at BERMS there was a passage of a weak warm front in the early morning (local time) of 10 July (Julian day 191). Similar to the passage of the weak cold front at Fraserdale, we will show the evolution of the warm front in the vertical cross-sections near BERMS. The 800 km long line along which the vertical cross-sections were taken is shown as line 2 in Fig. 1. In the cross-sections, BERMS is located at the 540 km point.

Figure 11 shows the vertical cross-sections of the θ, CO_2 and q fields (Figs. 11a, 11b and 11c, respectively) before the frontal passage at BERMS (day 191, 0 UT or day 190, 17 h local time), and Fig. 12 shows these fields after the frontal passage (day 192, 0 UT or day 191, 17 h local time). In Fig. 11a, the θ field shows the leading edge of the warm air (the warm front) at the 150 km point moving from left to right. The surface temperature minimum at the 200 km point is the result of reduced solar heating under the frontal cloud band. The sloping θ surfaces provide favourable neutral buoyancy for the frontal vertical transport. After the frontal passage, the temperature field shows little horizontal temperature gradient at the surface (Fig. 12a).

In the CO_2 field, Fig. 11b shows that at the 150 km point a band of air with a higher CO_2 concentration associated with the warm front reached the 500 mb level. The band structure shows sloping transport by frontal lifting from the surface and nearly

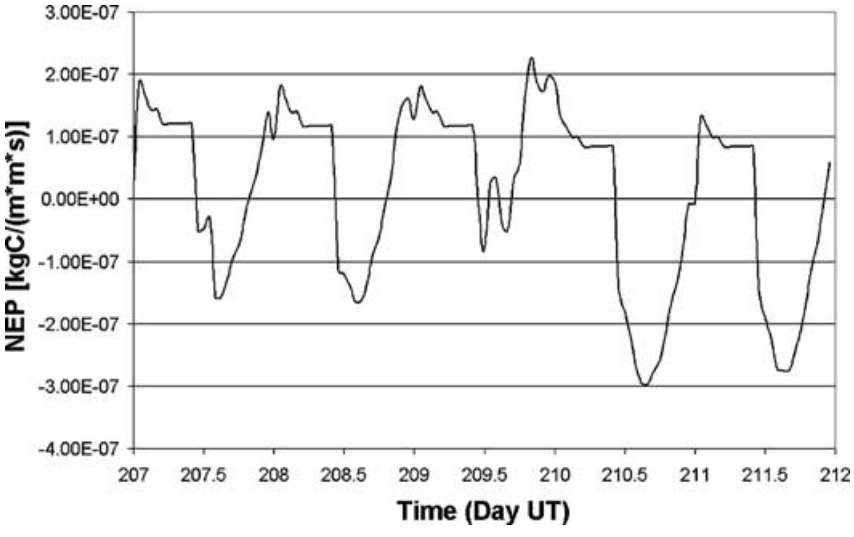

Fig 10. The evolution of the BEPS NEP flux at Fraserdale. Positive indicates a flux of CO_2 from the biosphere to the atmosphere.

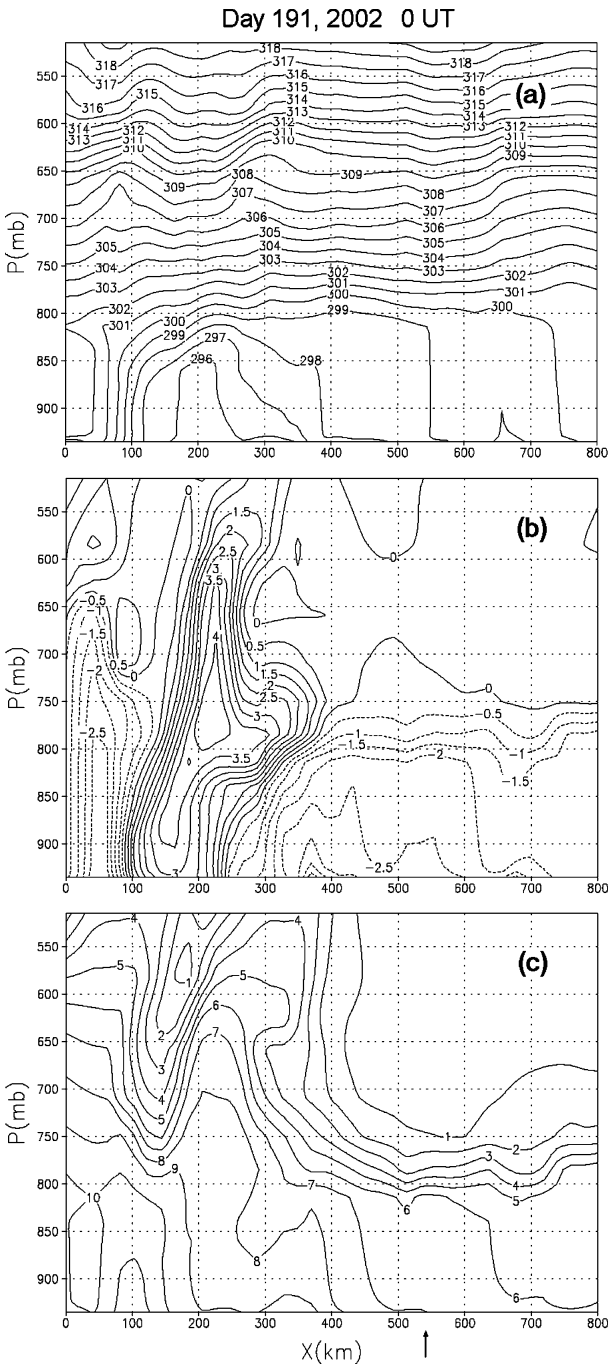

Fig 11. Vertical cross-sections of (a) potential temperature (K), (b) CO_2 (ppm) and (c) specific humidity q (g kg^{-1}), near BERMS (denoted by the arrow at 540 km) before the passage of the warm front.

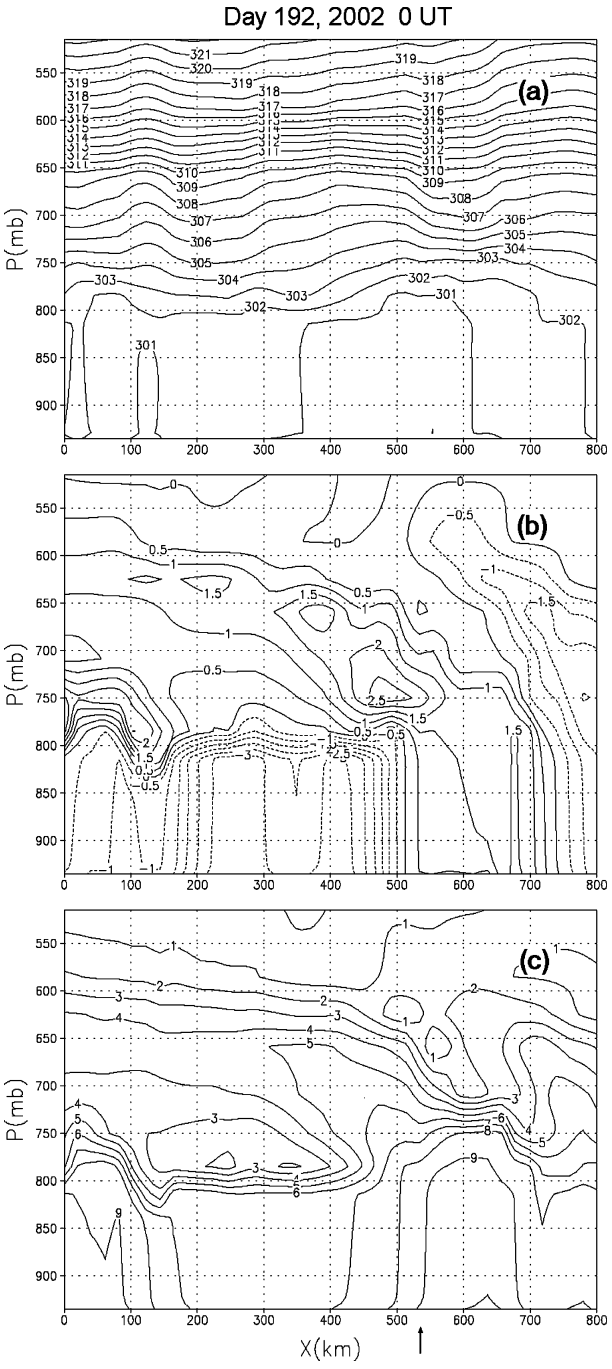

Fig 12. Vertical cross-sections of (a) potential temperature (K), (b) CO_2 (ppm) and (c) specific humidity q (g kg^{-1}), near BERMS (denoted by the arrow at 540 km) after the passage of the warm front.

vertical transport by the enhanced diabatic circulation induced by the frontal cloud band. This is another example of the interaction of the biosphere with the frontal cloud band. In the warm sector slightly behind the frontal band, the CO_2 field shows features of mesoscale vertical transport. The CO_2 was mixed to about the 650 mb level. While in the cold sector, the PBL at BERMS reached about 750 mb. The PBL height in the cold sector was almost uniform, indicating the weakness of mesoscale vertical motion between the PBL and the free troposphere.

Figure 12b shows the CO_2 concentration in the warm sector after the passage of the weak warm front at BERMS. In contrast to the cold sector, the CO_2 from the PBL is clearly mixing slantwise

into the free troposphere near BERMS up to about the 600 mb level. The strongly sloping transport coupled with the mesoscale variations in the CO_2 concentration result in the complex layered structures in the free troposphere near BERMS. There is a change in the sloping transport compared with the warm front in Fig. 11b. Clearly the upper airflow has shifted behind the front. As in the weak cold front simulation near Fraserdale, there are significant horizontal variations in CO_2 concentrations of the order of 5–10 ppm over a distance of about 100 km. Also notable in Fig. 12b is the region from about 200 km to 500 km, where the CO_2 in the PBL appears capped at the top of the PBL. This lack of mixing above the PBL is related to the moisture field presented next.

In Figure 11c, the q field shows the horizontal gradient of moisture from the moist air in the warm sector to the drier air in the cold sector. The vertical motion of the warm front and in the warm sector above the PBL, and the lack of vertical mixing at the top of the PBL in the cold sector, are both consistent with the modelled CO_2 field in Fig. 11b. In Fig. 12c, after the passage of the weak warm front, the slantwise transport of humidity across the PBL to the free troposphere is again evident near BERMS, similar to the CO_2 field. The region from about 200 km to 500 km has relatively low humidity. The drier air in this region is not favourable for cloud formation and diabatically forced circulation. This result is evident from the lack of exchange between the PBL and the free troposphere. Since CO_2 acts as a passive tracer in the atmosphere, this also explains the lack of vertical mixing of CO_2 in this region noted previously. Similarly, the "dry" cold sectors in these examples have little exchange between the PBL and the free troposphere. These results indicate that CO_2 mixing is strongly coupled to the mesoscale and synoptic scale transport and diabatic processes.

Again the model results can be compared qualitatively with the campaign aircraft vertical profiles of CO_2 concentrations at BERMS shown in Fig. 13. In Fig. 13, the surface tower CO_2 data are not plotted as the surface value of the profiles since the data are not yet available. Although the sequence of vertical profiles contains a great deal of detail, it is possible to delineate certain prominent features. A comparison of the afternoon profiles on 9 July (day 190, before the frontal passage) to the morning profiles on 10 July (day 191, after the frontal passage) shows that the front transported air with a lower CO_2 concentration below 850 mb and air with a higher CO_2 concentration above 800 mb to BERMS. These changes in the CO_2 concentrations of about 5 ppm are comparable to the modelled CO_2 variations near the front. Away from the warm front, the 10 July (day 191) afternoon aircraft profiles show the CO_2 concentration in the whole PBL to be increasing with time. This was the result of an advection of air in the warm sector with a horizontal CO_2 gradient of about 4 ppm over a distance of about 100 km (for a typical wind speed of 10 m s^{-1}). Another example of advection in the warm sector is the difference in the vertical profiles between the afternoon of 10 July (day 191) and the morning of 11 July (day 192). The morning profiles indicate air with a lower CO_2 concentration below 850 mb, as well as above 750 mb, compared with the previous afternoon profiles. These results are consistent with the modelled CO_2 field with horizontal mesoscale ($\sim$100 km) variations and vertically complex layered structures above the PBL. The layered structures are again evident in the afternoon profiles on 11 July (day 192).

The evolution of the simulated CO_2 flux at BERMS is presented in Fig. 14. The response of the CO_2 flux to the meteorological forcing is again evident in the day to day variations of the total daytime net flux. With BERMS in the cooler air on day 190, the total daytime net flux was -6.0×10^{-3} kg C m^{-2} (a strong draw-down of CO_2). Then, in the warm air sector on day 193, the BERMS area under cloudy condition became a CO_2 source with a total daytime net flux of 2×10^{-3} kg C m^{-2}. Thus the subsynoptic scale (or mesoscale) variations in the CO_2 flux are comparable to the synoptic scale variations in the Fraserdale case, Fig. 10.

Figures 10 and 14 showed the local picture of the CO_2 flux variations. It is also informative to show the temporal evolution of the spatial distribution of the CO_2 flux. Figures 15a , 15b and 15c show the BEPS CO_2 flux for 13 UT of day 190, 16 UT of day 190 and 0 UT of day 191 respectively. At 13 UT, day 190 in Fig. 15a, the CO_2 flux distribution showed strong draw-down in much of Ontario and Quebec where the local time was 9 h. While in Alberta and Saskatchewan, the daytime draw-down was beginning where the local time was 7 h. However, there were two prominent cloud bands which induced the two banded regions of CO_2 source fluxes, one arc shaped band in southern Alberta and Saskatchewan and one linear band from southern Alberta to northern Alberta. These bands of CO_2 source regions persisted for many hours and remained visible at 16 UT, day 190 in Fig. 15b. The linear CO_2 source region dissipated gradually (along with the cloud band) as the day progressed. In Fig. 15c at 0 UT, day 191, the linear band of CO_2 source had vanished and was replaced by a mixed pattern of sources and sinks. The arc-shaped band of CO_2 source in southern Saskatchewan persisted and showed propagation with time (with the movement of the cloud band). Also visible in southern Saskatchewan in Fig. 15c were other band-shaped regions of CO_2 sources and sinks. In general, the CO_2 flux variations due to meteorological conditions are typically larger than the CO_2 flux variations due to the heterogeneity in the vegetation.

The atmospheric CO_2 field contains the integrated history of the surface CO_2 flux forcing. This relationship is quite evident in the surface distribution of the atmospheric CO_2 concentration field for 0 UT, day 191, Fig. 16. There are banded features in the CO_2 field in Alberta and Saskatchewan corresponding to the banded regions of CO_2 source fluxes in Alberta and Saskatchewan (Fig. 15). Figure 15 showed that the linear-shaped CO_2 source region did not extend to the Alberta/Montana border. However, the banded feature in the CO_2 field showed that the air high in CO_2 was transported from the source region to the

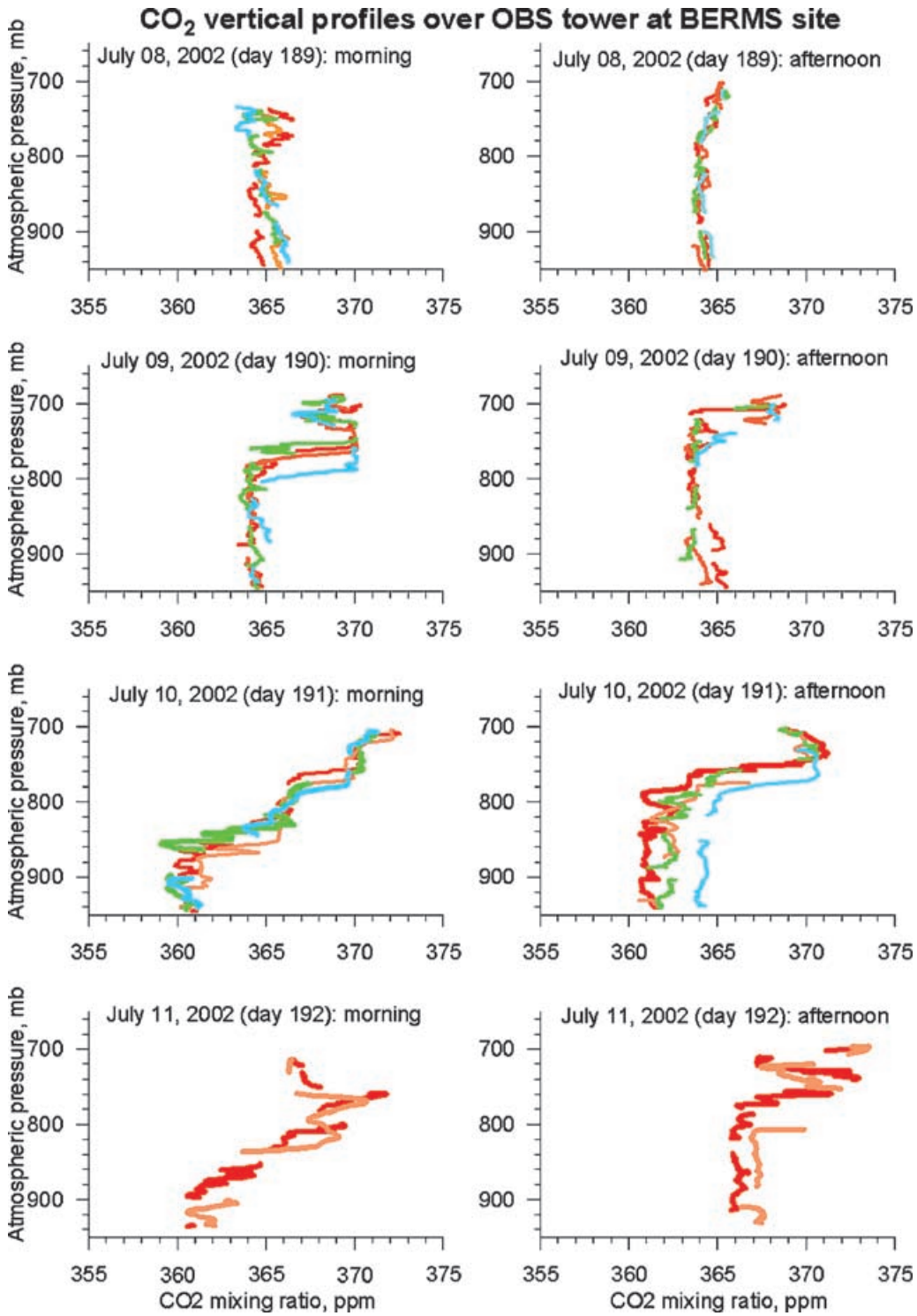

Fig 13. The sequence of aircraft vertical profiles for the July 2002 campaign. Each row shows the morning (from 15–17 UT) and afternoon (from 21–23 UT) vertical profiles for the same day. For each flight, there are up to four profiles corresponding to a sequence of ascents and descents, with each ascent or descent taking approximately 30 min. The profiles follow the rainbow colour sequence to denote the time sequence. Thus the first ascent is plotted in red, the following descent is plotted in orange, the next ascent in green and the final descent in blue. The uncertainty in the aircraft CO_2 measurement is about 0.3 ppm.

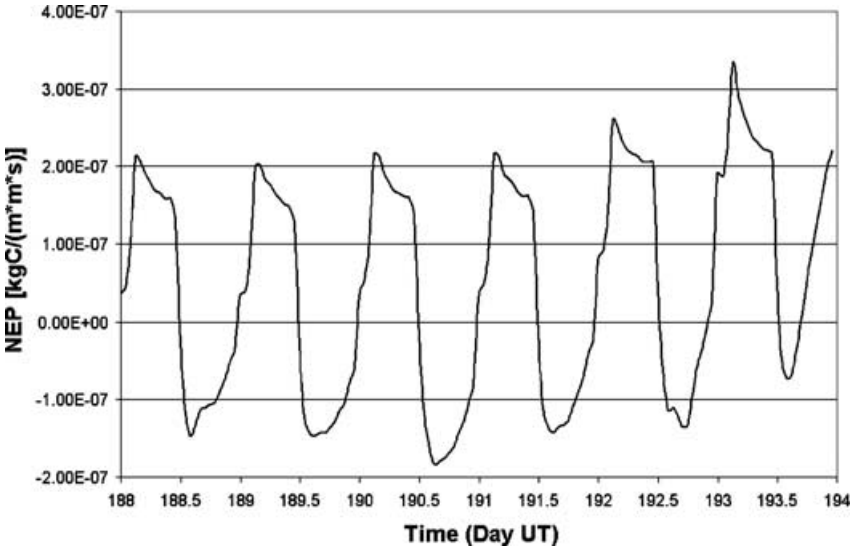

Fig 14. The evolution of the BEPS NEP flux at BERMS. Positive indicates a flux of CO_2 from the biosphere to the atmosphere.

Alberta/Montana border and then curved cyclonically into the centre of the low-pressure system at the Saskatchewan/Montana border. This is an illustration of the interaction between the atmospheric dynamics and the biosphere. The flow along the linear CO_2 source region allowed the air parcels to integrate the CO_2 source signals, resulting in the linear band of air enriched in CO_2 in Fig. 16. Similarly, the arc-shaped source region shown in Fig. 15 is associated with the arc-shaped CO_2 band in Fig. 16. This in fact is the weak warm frontal band discussed in the first part of this section (see Fig. 11b).

The relationship between biospheric flux inhomogeneity and the atmospheric CO_2 concentration is less direct. For example, the CO_2 flux over most of Ontario and Quebec (Fig. 15) shows persistent patterns of non-uniformity. In the absence of air motion, the near surface atmospheric CO_2 concentration would integrate the flux signal and display similar patterns of non-uniformity. However, as discussed above, the movement of air implied that the atmospheric CO_2 concentration field reflects the integrated history of flux patterns along the flow trajectories. Thus, Fig. 16 shows that the CO_2 concentration pattern is quite different from the biospheric flux inhomogeneity over Ontario and Quebec.

Simulation results for the Fraserdale and BERMS cases illustrate the importance of the interaction between atmospheric transport and the biospheric flux. In a model with an uncoupled atmosphere and biosphere (e.g. global inversion models with a neutral biosphere), the biosphere in the growing season will be producing a low concentration of CO_2, which the frontal circulation will transport upward efficiently. Thus, in an uncoupled mode, a frontal circulation like this in the summer will mix a low CO_2 concentration from the PBL to the free troposphere above. The uncoupling of the atmosphere and biosphere contributes to the error of the flux-transport covariance or the "rectifier effect". Whereas a model which properly couples the interactions of the baroclinic and diabatic processes with the biosphere should result in a more realistic "rectifier effect".

3.2.3 Vertical transport of CO_2 by a warm front. The model results for the weak frontal passages at Fraserdale and BERMS compared favourably with our intensive campaign observations. The natural question is what are the results for stronger frontal cases? Although the light aircraft used in our campaigns could not fly in conditions near a strong front, we can examine the model results for the more intense frontal case.

During the simulation of the July 2000 case, a strong warm front was found in western Canada. In Fig. 1, line 3 identifies the line along which a vertical cross-section of CO_2 was calculated. The vertical cross-section of CO_2 is shown in Fig. 17. This example of frontal transport is different from the warm front case of the 2002 BERMS campaign period (where CO_2-enriched air was transported to the free troposphere), illustrating a range of possible couplings between the atmosphere and the biosphere in the presence of synoptic scale forcing. Due to the slantwise flow at the warm front, the cloud radiative forcing is reducing the CO_2 uptake in the region of cold air ahead of the front. The cold air enriched in CO_2 is under stable stratification and thus remains near the surface. The slantwise upward flow of warm air with a low CO_2 concentration is quite evident. Frontal transport reached up to the 300 mb level in this case. Thus frontal mixing can transport surface CO_2 to the middle and upper troposphere. The importance of the interaction between the atmosphere and the biosphere is clearly demonstrated in this case in terms of its effect on the covariance between these two components.

3.3. Model simulations of mesoscale processes

In the comparison of the model results with the aircraft measurements (Section 3.1), it was noted that there are different exchange processes across the top of the PBL working on

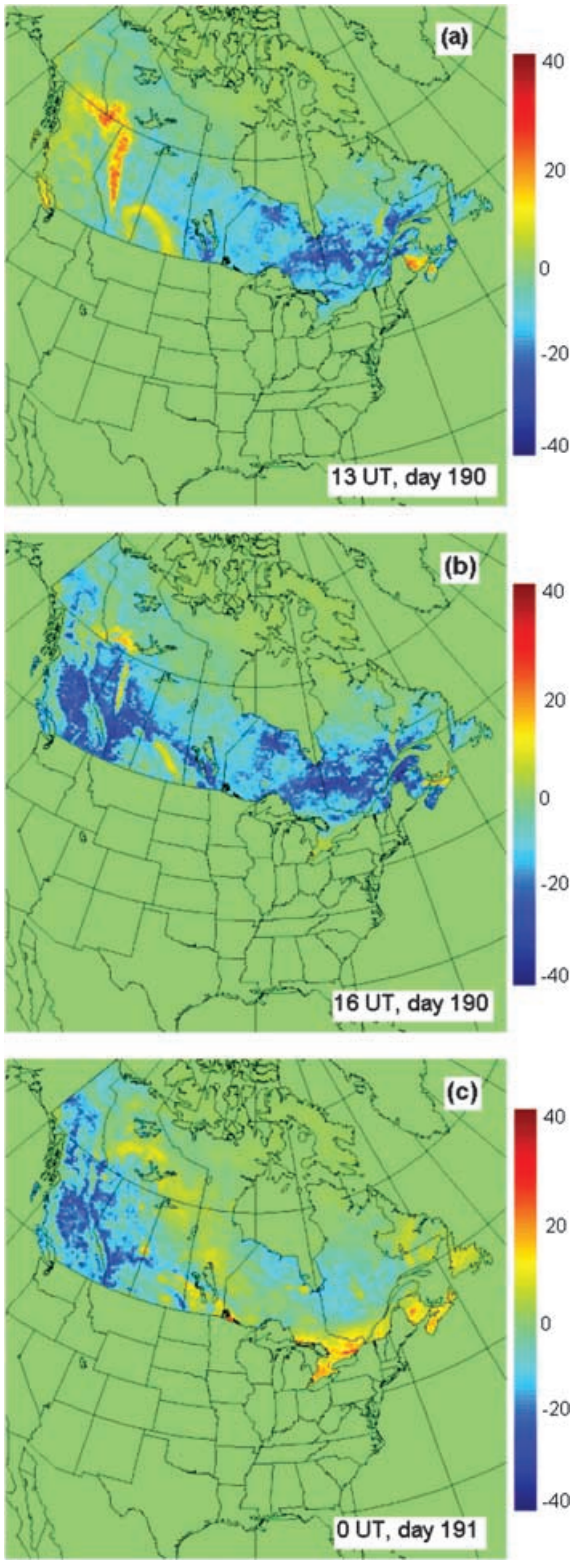

Fig 15. The evolution of the spatial distribution of the NEP fluxes for (a) 13 UT, day 190, (b) 16 UT, day 190 and (c) 0 UT, day 191. The contours are in units of 10^{-8} kg C m^{-2} s^{-1}. Positive indicates a flux of CO_2 from the biosphere to the atmosphere.

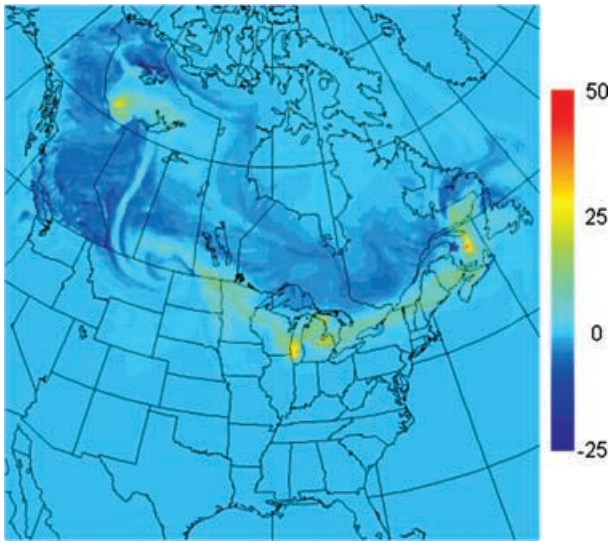

Fig 16. The model horizontal distribution of CO_2 (ppm) at the 15 m level for 0 UT, 11 July 2002 (day 191).

different days at Fraserdale under different air masses. Then, the simulation results in Section 3.2 showed that in the warm sector, the CO_2 field commonly contained mesoscale variations and the variations were transported into the lower free troposphere by mesoscale circulation. While in the cold sector, the CO_2 variations were weaker and there were little mesoscale exchange between the PBL and the free troposphere.

The cause of the mesoscale circulation is similar to the case for synoptic scale circulation. In the presence of a horizontal temperature gradient (baroclinicity), thermally direct circulation is induced so that warm air rises and cool air sinks. In the synoptic scale case, with $\Delta\theta \sim 10$ K over $\Delta x \sim 1000$ km, the circulation induced leads to the formation of the familiar baroclinic wave with warm front, cold front, warm sector and cold sector. For mesoscale anomalies, Chan and Cho (1989) showed that small potential temperature anomalies of typically $\Delta\theta \sim 1$ K over $\Delta x \sim 100$ km has a similar temperature gradient as the synoptic scale case. Thus mesoscale θ anomalies, by their mesoscale baroclinicity, can induce significant mesoscale circulation. The relationship between the horizontal scale L_x to the vertical scale L_z in the adiabatic case is given by

$$L_z \sim \left(\frac{f}{N}\right) L_x,$$

where f ($\sim 10^{-4}$ s^{-1}) is the Coriolis parameter and N ($\sim 10^{-2}$ s^{-1}) is the Brunt–Väisälä frequency. Due to their small horizontal scale, mesoscale anomalies typically have a smaller vertical scale ($\sim$1 km) and shorter time scale ($\sim$1 day) than synoptic scale circulation.

There are many possible causes of mesoscale anomalies, including variations in topography, differences in vegetation (albedo, roughness length, etc.), land–water contrast, cloud

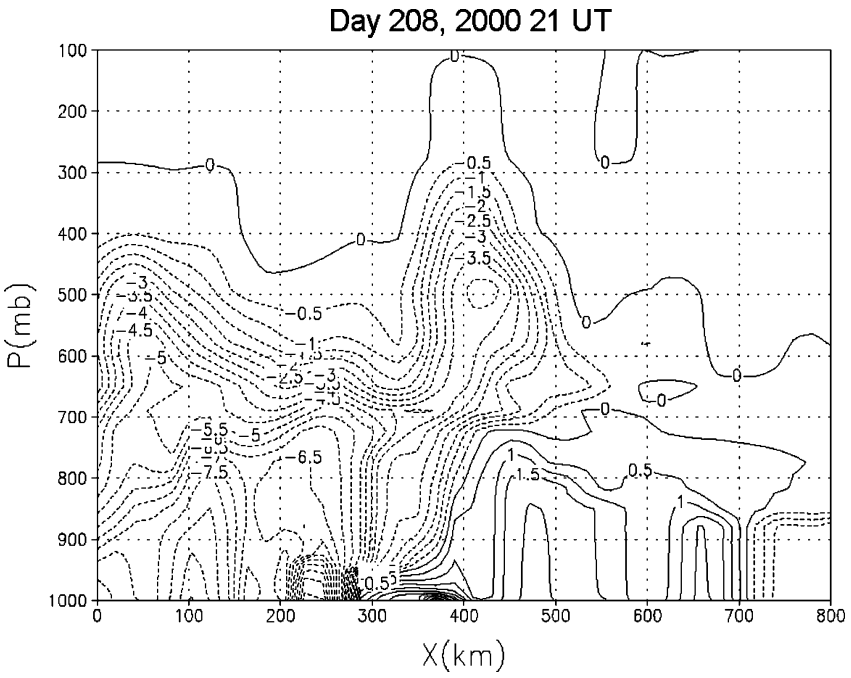

Fig 17. Vertical cross-section of the CO_2 field (ppm) for a stronger warm front. The warm sector is to the left of the warm front.

coverage, soil moisture variations, etc. Thus mesoscale anomalies and mesoscale circulation can be common features in the PBL dynamics. However, Chan and Cho (1989) showed that in the presence of diabatic heating in the free troposphere (cloud formation), mesoscale anomalies could extend into the mid-troposphere. This can explain the model results that in the warm sector, with the large-scale rising motion and diabatic cloud formation occurring, the mesoscale circulation extends into the free troposphere. This results in exchange of air between the PBL and the free troposphere. While typically in the cold sector with subsidence and a cloud-free troposphere, the mesoscale circulation is confined to within the PBL and a strong gradient of CO_2 concentration is built up between the PBL and the free troposphere (see Fig. 8b). Thus, baroclinicity on the mesoscale plays an important role in the interaction of atmospheric transport and the biospheric CO_2 flux. Low-resolution atmospheric circulation models do not resolve the mesoscale processes and may not capture the role of the mesoscale processes in the interaction.

The mesoscale θ anomalies above the PBL are quite evident as wave-like features in the warm sectors and are absent in the cold sectors in Figs. 7, 8, 11 and 12. The relationship between the mesoscale θ anomalies and CO_2 and q are evident in these respective figures.

4. Conclusions

In order to decompose the atmospheric CO_2 measurements from a network of surface monitoring stations in terms of the terrestrial carbon sources and sinks, we need to clearly identify the processes by which the biospheric flux of CO_2 is communicated to the troposphere. In this study, we have addressed part of this issue by demonstrating the significance of the impact of synoptic scale and mesoscale atmospheric processes have on a regional distribution of atmospheric CO_2. As part of the overall research strategy, we have developed a coupled regional atmospheric model (MC2) and a biospheric CO_2 flux model (BEPS). BEPS is driven by the meteorological fields and radiative flux from MC2. In turn, MC2 transports CO_2 in the atmosphere as a tracer with surface fluxes from BEPS. Comparison of the model results and observations at Fraserdale showed that the model could realistically simulate the diurnal exchange processes between the biosphere and the atmosphere. The model has difficulties with small-scale processes and shallow surface layers that cannot be resolved by MC2.

Model simulation showed the importance of the synoptic scale exchange processes. Coupling of the atmosphere to the biosphere produced gradients in the surface CO_2 concentration in response to the modulation of the photosynthesis by cloud cover; CO_2 concentration is elevated near frontal regions and other regions with cloudy conditions. Model results also showed that frontal transports provided deep mixing of surface CO_2 to the mid to upper troposphere, including elevated CO_2 air near the fronts. Warm sector air with large-scale lifting and favourable conditions for diabatic heating can transport surface CO_2 to the mid-troposphere.

On shorter time scales, mesoscale processes can produce variations in the CO_2 concentration up to ~5–10 ppm on space and time scales of 100 km and 1 day, respectively. Furthermore, mesoscale circulation enhanced by diabatic heating in the warm sector can transport PBL CO_2 into the lower troposphere.

Indeed, synoptic and mesoscale transport (horizontal and vertical) processes of CO_2 are comparable to the effect produced by local biospheric fluxes. The model-simulated mesoscale and synoptic scale CO_2 concentration variability are comparable to the variability observed in intensive campaign aircraft profiles at Fraserdale and BERMS. The aircraft observations might contain other factors such as fossil fuel CO_2 and other biospheric processes not simulated by the model (e.g. long-range transport from the USA). These factors might explain these differences between the model results and observations. Further studies are needed to quantify the role of mesoscale and synoptic scale processes in the mid-troposphere to understand how atmospheric CO_2 is transported to the monitoring stations once it leaves the PBL.

Our model simulations have highlighted those cases in which the transport processes from the PBL region to the free troposphere appeared unambiguous. The real atmosphere is of course much more complex. It is possible in other cases to have clear sky conditions in the warm sector air mass and cloudy conditions in the cold sector air mass. There could be other baroclinic processes, including fast-moving short waves, comma lows, etc. Thus the interaction of synoptic scale and mesoscale transport and biospheric fluxes is highly dependent on the atmospheric conditions. It is clear that it is a complex problem to model the full interaction or coupling between atmospheric transport and biospheric fluxes.

The results of our study, though limited to a certain extent, suggest the importance of synoptic scale and mesoscale processes in the formation of variability in CO_2 concentration and transport from continental source–sink regions to the free troposphere and subsequently the whole atmosphere. Therefore, including these processes in global carbon cycle inversion models should yield more realistic rectifier effects and provide more reasonable estimates of the missing sink. Correct transport of CO_2 fluxes is one important factor in minimizing the errors of inversion estimates of CO_2 sources and sinks.

5. Acknowledgments

We thank A. Scott Denning (Colorado State University) for helpful discussions about these results. We thank L. Huang (Meteorological Service of Canada) and S. Murayama (National Institute of Advanced Industrial Science and Technology, Japan) for the many useful discussions and careful reviews of this manuscript. We also thank I. Enting (CSIRO) and K. Gurney (Colorado State University) for their comments and suggestions; they were very helpful and made this paper clearer. We are grateful to G. Mo (University of Toronto) for assisting in the modifications of the BEPS model. The modelling work was supported by the Canadian Foundation for Climate and Atmospheric Sciences (CFCAS) and the measurements were supported by the Panel of Energy Research and Development (PERD).

References

Bakwin, P. S., Tans, P. P., Zhao, C., Ussler, W. and Quesnell, E. 1995. Measurements of carbon dioxide on a very tall tower. *Tellus* **47B**, 535–549.

Bakwin, P. S., Tans, P. P., Hurst, D. F. and Zhao, C. 1998. Measurements of carbon dioxide on very tall towers: results of the NOAA/CMDL program. *Tellus* **50B**, 401–415.

Benoit, R., Cote, J. and Mailhot, J. 1989. Inclusion of a TKE boundary layer parameterization in the Canadian regional finite-element model. *Mon. Weather Rev.* **117**, 1726–1750.

Benoit, R., Desgagne, M., Pellerin, P., Pellerin, S. and Chartier, Y. 1997. The Canadian MC2: a semi-Lagrangian, semi-implicit wideband atmospheric model suited for fine scale process studies and simulation. *Mon. Weather Rev.* **125**, 2382–2415.

Chan, D. and Cho, H. R., 1989. Meso-β scale potential vorticity anomalies and rainbands. Part I: adiabatic dynamics of the potential vorticity anomalies. *J. Atmos. Sci.* **46**, 1713–1723.

Chen, J. M., 1996a. Optically-based methods for measuring seasonal variation of leaf area index in boreal conifer stands. *Agric. Forest Meteorol.* **80**, 135–163.

Chen, J. M., 1996b. Canopy architecture and remote sensing of the fraction of photosynthetically active radiation absorbed by boreal conifer forests. *IEEE Trans. Geosci. Remote Sens.* **34**, 1353–1368.

Chen, J. M. and Cihlar, J., 1996. Retrieving leaf area index of boreal conifer forest using Landsat TM images. *Remote Sens. Environ.* **55**, 153–162.

Cihlar, J., Beaubien, J., Latifovic, R. and Simard, G. 1999. *Land Cover of Canada 1995, Version 1.1*. Digital data set documentation, Natural Resources Canada, Ottawa, Ontario. ftp://ftp2.ccrs.nrcan.gc.ca/ftp/ad/EMS/landcover95/.

Cihlar, J., Chen, J. M. and Li, Z. 1997. Seasonal AVHRR multichannel datasets and products for studies of surface-atmosphere interactions. *J. Geophys. Res.* **102**, 29 625–29 640.

Deardorff, J. W., 1978. Efficient prediction of ground surface temperature and moisture with the inclusion of a layer of vegetation. *J. Geophys. Res.* **83**, 1889–1903.

Denning, A. S., Fung, I. Y. and Randall, A. D. 1995. Latitudinal gradient of atmospheric CO_2 due to seasonal exchange with land biota. *Nature* **376**, 240–243.

Denning, A. S., Collatz, J. G., Zhang, C., Randall, D. A., Berry, J. A., et al, 1996a. Simulations of terrestrial carbon metabolism and atmospheric CO_2 in a general circulation model. Part 1: Surface carbon fluxes. *Tellus* **48B**, 521–542.

Denning, A. S., Randall, D. A., Collatz, G. J. and Sellers, P. J. 1996b. Simulations of terrestrial carbon metabolism and atmospheric CO_2 in a general circulation model. Part 2: Spatial and temporal variations of atmospheric CO_2. *Tellus* **48B**, 543–567.

Denning, A. S., Takahashi, T. and Friedlingstein, P. 1999. Can a strong atmospheric CO_2 rectifier effect be reconciled with a "reasonable" carbon budget? *Tellus* **51B**, 249–253.

Fouquart, Y. and Bonnel, B., 1980. Computations of solar heating of the earth's atmosphere: a new parameterization. *Contrib. Atmos. Phys.* **53**, 36–62.

Gal-Chen, T. and Somerville, R., 1975. On the use of a coordinate transformation for the solution of the Navier–Stokes equations. *J. Comput. Phys.* **17**, 209–228.

Garand, L., 1983. Some improvements and complements to the infrared emissivity algorithm including a parameterization of the absorption in the continuum region. *J. Atmos. Sci.* **40**, 230–244.

Gurney, R. K., Law, R. M., Denning, A. S., Rayner, P. J., Baker, D., et al, 2002. Towards robust regional estimates of CO_2 sources and sinks using atmospheric transport models. *Nature* **415**, 626–630.

Higuchi, K., Worthy, D., Chan, D. and Shashkov, A. 2003. Regional source/sink impact on diurnal, seasonal and inter-annual variations in atmospheric CO_2 at a boreal forest site in Canada. *Tellus* **55B**, 115–125.

Kuo, H. L., 1974. Further studies of the parameterization of the influence of cumulus convection on large-scale flow. *J. Atmos. Sci.* **46**, 545–564.

Liu, J., Chen, J. M., Cihlar, J. and Park, W. M. 1997. A process-based boreal ecosystem productivity simulator using remote sensing inputs. *Remote Sens. Environ.* **62**, 158–175.

Liu, J., Chen, J.M., Cihlar, J. and Chen, W. 2002. Net primary productivity mapped for Canada at 1-km resolution, *Global Ecol. Biogeog.* **11**, 115–129.

Mailhot, J., 1994. *The Regional Finite-element (RFE) Model Scientific Description. Part 2: Physics*. (Available from RPN, 2121 Trans-Canada, Dorval, QC H9P 1J3, Canada.)

Mailhot, J., Chouinard, C., Benoit, R., Roch, M., Verner, G., Cote, J. and Pudykiewicz, J. 1989. Numerical forecasting of winter coastal storms during CASP: evaluation of the regional finite-element model. *Atmos. Ocean* **27**, 27–58.

Running, S. W. and Coughlan, J. C., 1988. A general model of the forest ecosystem processes for regional applications I: hydrological balance, canopy gas exchange and primary production processes. *Ecol. Model.* **42**, 125–154.

Shields, J. A., Tarnocai, C., Valentine, K. W. G. and MacDonald, K. B. 1991. *Soil Landscapes of Canada: Procedures Manual and Userʹs Handbook*. Agriculture Canada Publication 1868/E, Ottawa, Canada.

Stull, R. B., 1993. *An Introduction to Boundary Layer Meteorology*. Kluwer Academic Publishers, Dordrecht.